Proceedings of the 7th RSI
International Conference on Robotics and Mechatronics (ICRoM 2019)
November 20-21, 2019, Tehran, Iran

Dynamics Modeling and Position Control of a Robotic Carrier for Solar Panel Cleaning System

F. Hajiahmadi[1], P. Zarafshan*[1], M. Dehghani[2], S. Ali A. Moosavian[3], S. R. Hassan-Beygi[1]
[1]Department of Agro-Technology, College of Aburaihan, University of Tehran, Tehran, Iran
[2] Department of Food Technology, College of Aburaihan, University of Tehran, Tehran, Iran
[3]Dept. of Mechanical Engineering, K. N. Toosi Univ. of Technology, Tehran, Iran
Corresponding Author: p.zarafshan@ut.ac.ir

***Abstract*— In this paper, modeling and control of a robotic carrier for the cleaning system of solar power plants is presented. Since solar panels are placed at natural environments, there is always a problem of dust accumulation on the panels, which results in absorbed energy reduction. Hence, robotic cleaners can be used for solar panels. For relocation of such cleaning robots between solar panel rows, an automated carrier mechanism is required. Hence, a robotic system for cleaner displacement is introduced, and its dynamic modeling and control are presented. To this end, the kinematic characteristics of the robot are introduced, and the dynamic model is derived based on the energy methods. For model validation, the robot is built and simulated in ADAMS, and the results are compared. Finally, the dynamic model is used to design a position controller. The controlled system is simulated using a MATLAB and ADAMS co-simulation. The results show that the derived model and the designed controller are precise and practical.**

Keywords: solar panel cleaning robot; AGV; dynamic modeling; simulation; PID.

I. INTRODUCTION

Solar power is one the most important energy sources in the world. One major problem that reduces energy efficiency of solar panels is the dust accumulation on the panels. This problem gets worse where the solar power plant is placed near agricultural terrains, mine structures and other polluted areas. For instance, the agricultural dusts can be blown to nearby areas, and form a thick layer of dust, which is specifically important for AgroPhotoVoltaic (APV) systems, in which solar panels are placed at the agricultural sites. These systems are used where land is scarce and very valuable; and also, where the plants need to have a shelter or a partial shadow against the direct sun light, [1, 2].

In order to avoid deficiency, the panels must be cleaned in regular plans. This cleaning is a difficult maintenance task for large power plants with many long rows of solar panels, considering the high risks of electric shock for the workers and the risks of damaging the panels. Furthermore, due to the very wide surface area of the panels, the quality of cleaning is usually low, and sometimes a lot of water is required, or heavy machinery is used, as depicted in Fig. 1. Specifically, where very wide panels are placed at higher heights, specific machinery is required, which might damage the panels, [3, 4].

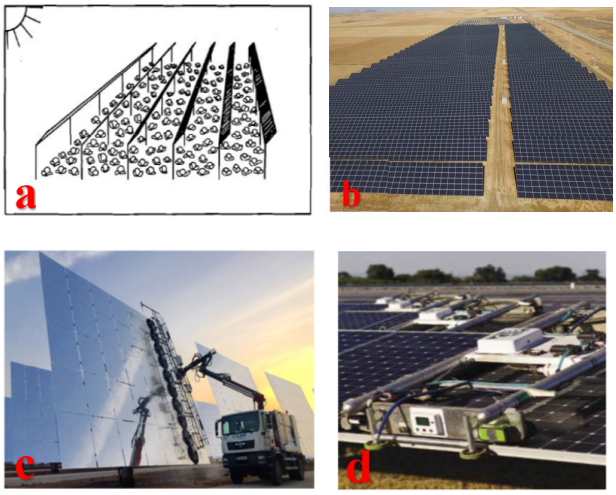

Fig. 1 Solar Power Plants and Cleaning of them; (a) an APV system, [5]; (b) Sollar Craneir Parsian in Hamedan, [6]; (c) cleaning with heavy fossil fuel machinery, [7]; (d) a robotic cleaning system, [8];

Exploiting light, small and smart robotic cleaning systems, the maintenance process can be done automatically or remotely controlled, with higher qualities and without human safety risks. Furthermore, longer lifecycles of panels and less water consumption may be achieved. Using such automatic systems on regular basis, dust, snow and birds faeces and corps can be removed. Even in dry areas, studies have shown that up to 15% of energy loss due to the mentioned problems, [9, 10].

Many designs have been presented for solar panel cleaning robots, [11]. Some robots can move on the panels, [12], while some others move on the ground or rails and clean the panels all along their path, [13, 14]. Fig. 1.a shows an APV plant, where the agricultural activities can increase the dust in the area, [15]. Fig. 1.c depicts a cleaning machine, which is carried and controlled by a truck. In order to reduce the chance of damaging, the manipulators must be soft [16-18]. For robotic systems, the use of continuum manipulators seems to be suitable for this method, [19, 20]. Fig. 1.d depicts robots moving on the panels. Such robots need to be light, and have proper wheels which do not damage the panel surfaces. Typically, the required components can be placed in a single carrier; otherwise, a series of carriers would be required, [21].

978-1-7281-6604-9/19/$31.00 ©2019 IEEE

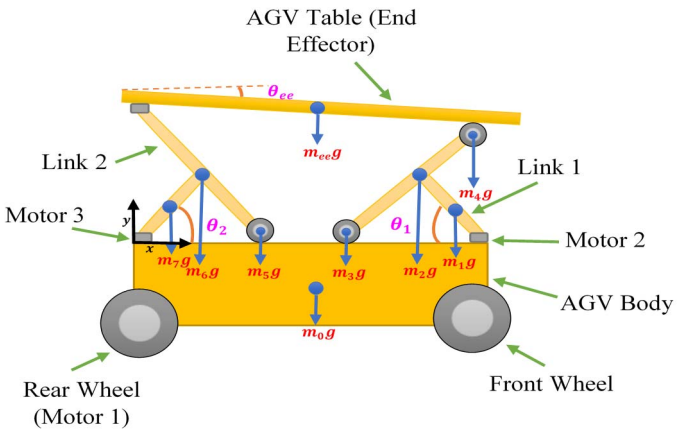

Fig. 2 Schematic of the system with geometric properties

As depicted in Fig. 1, in most power plants, the panels are placed in rows of tens or hundreds of meters. Typically, each row of panels has its own cleaning robot. The main reason is the difficulty of robot transportation between the rows. To overcome this problem, a robotic carrier system can be used, to transfer the cleaner between the rows, [22, 23]. As depicted in Fig. 1, the rows are typically placed adjacently, and it is possible to place passages besides the rows for such a robot carrier. In this paper, a robotic carrier system is studied, which can move on a railed path, and can transfer the cleaning robot between panel rows.

In this paper, as a part of the initial design of the robotic maintenance system, the kinematic and dynamic models of the carrier robot are presented. In section II, the initial design of the robotics system is briefly presented. Afterward, kinematic and kinetic models of the robot are presented. In section III, the derived model is validated, using ADAMS software. For the validation, four case studies are presented and the results are compared. After the validation, in section IV, a controller is designed for the robot. The robot control is simulated using MATLAB Simulink and ADAMS co-simulation. The results show that the proposed system is capable for the desired tasks. These results are also used for finalizing the design, before the manufacturing of the robotic system.

II. Dynamic Modeling

In this section, the dynamic modeling of the robot is presented. The kinematics variables are introduced in Fig. 2. The robot has three degrees of freedom, including moving forward and backward on a rail; and two degrees for height adjustment of the front and rear scissors. Based on the motor placement, (x, θ_1, θ_2) can be chosen as the inputs of the control system, or as the general coordinates. Regarding the final task, the position of the table -considered as the robot End Effector- the control output or the general coordinates can be considered as (x_{ee}. y_{ee}. θ_{ee}).

A. System kinematics

Using the kinematics shown in Fig. 2, $x_{ee}.y_{ee}.\theta_{ee}$ are derived as in (1), where, l_{ee} is the table length; a is the length of the robot (distance between motor 2 and motor 3 axes); l_1 and l_2 are lengths of links 1 and 2 respectively; θ_1 and θ_2 are respectively the angle of the front and rear scissors. For abbreviation, $\sin\theta_i$ and $\cos\theta_i$ are represented as s_i and c_i.

$$x_{ee} = x + \frac{l_{ee}c_{ee}}{2} = x + \frac{l_{ee}a}{4\sqrt{(2l_1s_1 - 2l_2s_2)^2 + a^2}}$$
$$y_{ee} = 2l_2s_2 + \frac{l_{ee}s_{ee}}{2} = 2l_2s_2 + \frac{l_{ee}(l_1s_1 - l_2s_2)}{2\sqrt{(2l_1s_1 - 2l_2s_2)^2 + a^2}} \quad (1)$$
$$\theta_{ee} = \tan^{-1}\left(\frac{2l_1s_1 - 2l_2s_2}{a}\right)$$

For kinetic and kinematic modeling, the position of mass centers and orientation of all parts are required. Hence, using the geometry introduced in Fig. 2, orientation and center position of all robot parts are as follows. It should be noted that the robot body is referred to as link 0.

$$\begin{aligned}
&x_0 = 0.5a + x && y_0 = 0 && \theta_0 = 0\\
&x_1 = x + a - 0.5l_1c_1 && y_1 = 0.5l_1s_1 && \theta_1 = \pi - \theta_1\\
&x_2 = x + a - l_1c_1 && y_2 = l_1s_1 && \theta_2 = \theta_1\\
&x_3 = x + a - 2l_1c_1 && y_3 = 0 && \theta_3 = 0\\
&x_4 = a + x && y_4 = 2l_1s_1 && \theta_4 = 0\\
&x_5 = x + 2l_2c_2 && y_5 = 0 && \theta_5 = 0\\
&x_6 = x + l_2c_2 && y_6 = l_2s_2 && \theta_6 = \pi - \theta_2\\
&x_7 = x + 0.5l_2c_2 && y_7 = 0.5l_2s_2 && \theta_7 = \theta_2
\end{aligned} \quad (2)$$

Using the derivatives of (2) with respect to the general coordinates (x, θ_1, θ_2), the Jacobian matrices for x,y position of links are derived as follows, where v refers to linear velocity.

$$J_{v_0} = \begin{bmatrix} 1 & 0 & 0 \\ 0 & 0 & 0 \end{bmatrix} \qquad J_{v_1} = \begin{bmatrix} 1 & 0.5l_1s_1 & 0 \\ 0 & 0.5l_1c_1 & 0 \end{bmatrix}$$
$$J_{v_2} = \begin{bmatrix} 1 & l_1s_1 & 0 \\ 0 & l_1c_1 & 0 \end{bmatrix} \qquad J_{v_3} = \begin{bmatrix} 1 & 2l_1s_1 & 0 \\ 0 & 0 & 0 \end{bmatrix}$$
$$J_{v_4} = \begin{bmatrix} 1 & 0 & 0 \\ 0 & 2l_1c_1 & 0 \end{bmatrix} \qquad J_{v_5} = \begin{bmatrix} 1 & 0 & -2l_2s_2 \\ 0 & 0 & 0 \end{bmatrix} \quad (3)$$
$$J_{v_6} = \begin{bmatrix} 1 & 0 & -l_2s_2 \\ 0 & 0 & l_2c_2 \end{bmatrix} \qquad J_{v_7} = \begin{bmatrix} 1 & 0 & -\frac{l_2}{2}s_2 \\ 0 & 0 & \frac{l_2}{2}c_2 \end{bmatrix}$$

And for the End Effector, the Jacobian matrix is

$$\mathbf{J}_{v_{ee}} = \begin{bmatrix} 1 & \frac{l_1l_{ee}c_1\beta}{a^2\lambda^3} & \frac{l_2l_{ee}c_2\beta}{a^2\lambda^3} \\ 0 & \frac{l_1l_{ee}c_1}{a\lambda} - \frac{l_1l_{ee}c_1\beta^2}{a^3\lambda^3} & 2l_2c_2 - \frac{l_2l_{ee}c_2}{a\lambda} - \frac{l_2l_{ee}c_2\beta^2}{a^3\lambda^3} \end{bmatrix} \quad (4)$$

where: $\lambda = \sqrt{\frac{(2l_1s_1 - 2l_2s_2)^2}{a^2} + 1}$, and $\beta = 2l_1s_1 - 2l_2s_2$

Likewise, the Jacobian matrices for orientations of the links are derives in (5), where, ω refers to angular speeds.

$$\begin{aligned}
&\mathbf{J}_{\omega_0}=[0\ \ 0\ \ 0] && \mathbf{J}_{\omega_1}=[0\ \ -1\ \ 0]\\
&\mathbf{J}_{\omega_2}=[0\ \ 1\ \ 0] && \mathbf{J}_{\omega_3}=[0\ \ 0\ \ 0]\\
&\mathbf{J}_{\omega_4}=[0\ \ 0\ \ 0] && \mathbf{J}_{\omega_5}=[0\ \ 0\ \ 0]\\
&\mathbf{J}_{\omega_7}=[0\ \ 0\ \ 1] && \mathbf{J}_{\omega_6}=[0\ \ 0\ \ -1]\\
&\mathbf{J}_{\omega_{ee}}=\begin{bmatrix}0 & \frac{2l_1c_1}{a\lambda^2} & -\frac{2l_2c_2}{a\lambda^2}\end{bmatrix}
\end{aligned} \tag{5}$$

Using (3)-(5), the mass center velocity v_i and angular velocity ω_i of each link can be obtained by

$$\begin{aligned}
&\mathbf{v}_i=\mathbf{J}_{v_i}\dot{\mathbf{q}}\\
&\boldsymbol{\omega}_i=\mathbf{J}_{\omega_i}\dot{\mathbf{q}}
\end{aligned} \tag{6}$$

Using the Jacobian matrices, the velocities can be determined as (7) for the table and (8) for other parts, to present a complete kinematic model.

$$\begin{aligned}
&\dot{x}_{ee}=\dot{x}-\frac{(l_1l_{ee}c_1\dot{\theta}_1+l_2l_{ee}c_2\dot{\theta}_2)\beta}{a^2\lambda^3}\\
&\dot{y}_{ee}=(\dot{\theta}_1l_1c_1-\dot{\theta}_2l_2c_2)\frac{l_{ee}^2\beta^2}{a^4\lambda^4}+2l_2c_2\dot{\theta}_2\\
&\dot{\theta}_{ee}=\frac{2l_1\dot{\theta}_1c_1-2l_2\dot{\theta}_2c_2}{a\lambda^2}
\end{aligned} \tag{7}$$

It should be noted that the inertia of the wheels are negligible compared to other masses, and their angular speed are also small. Hence, $\dot{\theta}_3.\ \dot{\theta}_4.\ \dot{\theta}_5$ are not important for dynamic modeling. However, in (8), r_w is the wheels radius.

$$\begin{aligned}
&\dot{x}_0=\dot{x} && \dot{y}_0=0 && \dot{\theta}_0=0\\
&\dot{x}_1=\dot{x}+0.5l_1s_1\dot{\theta}_1 && \dot{y}_1=0.5l_1c_1\dot{\theta}_1 && \dot{\theta}_1=-\dot{\theta}_1\\
&\dot{x}_2=\dot{x}+l_1s_1\dot{\theta}_1 && \dot{y}_2=l_1c_1\dot{\theta}_1 && \dot{\theta}_2=\dot{\theta}_1\\
&\dot{x}_3=\dot{x}+2l_1s_1\dot{\theta}_1 && \dot{y}_3=0 && \dot{\theta}_3=2l_1s_1\dot{\theta}_1\\
&\dot{x}_4=\dot{x} && \dot{y}_4=2l_1c_1\dot{\theta}_1 && \dot{\theta}_4\simeq 0\\
&\dot{x}_5=\dot{x}-2l_2s_2\dot{\theta}_2 && \dot{y}_5=0 && \dot{\theta}_5=-2l_2s_2\dot{\theta}\\
&\dot{x}_6=\dot{x}-l_2s_2\dot{\theta}_2 && \dot{y}_6=l_2c_2\dot{\theta}_2 && \dot{\theta}_6=-\dot{\theta}_2\\
&\dot{x}_7=\dot{x}-0.5l_2s_2\dot{\theta}_2 && \dot{y}_7=0.5l_2c_2\dot{\theta}_2 && \dot{\theta}_7=\dot{\theta}_2
\end{aligned} \tag{8}$$

B. System dynamics

Based on Lagrangian formulation, the dynamic model can be derived. The kinetic energy can be represented in matrix form, as (9).

$$\text{K.E.}=\frac{1}{2}\dot{\mathbf{q}}^T\mathbf{M}\dot{\mathbf{q}}=\frac{1}{2}\dot{\mathbf{q}}^T[\textstyle\sum_{i=1}^{n}(m_i\mathbf{J}_{v_i}{}^T\mathbf{J}_{v_i}+\mathbf{J}_{\omega_i}{}^T\mathrm{I}_{ci}\mathbf{J}_{\omega_i})]\dot{\mathbf{q}} \tag{9}$$

The positive definite inertia matrix **M** is achieved using (10), in which, I_{ci} is the second moment of inertial and m_i the mass of the i^{th} link. The general coordinates are chosen as $\mathbf{q}=[x\quad \theta_1\quad \theta_2]^T$, [24, 25].

$$\mathbf{M}=\textstyle\sum_{i=1}^{n}(m_i\mathbf{J}_{v_i}{}^T\mathbf{J}_{v_i}+\mathbf{J}_{\omega_i}{}^T\mathrm{I}_{c_i}\mathbf{J}_{\omega_i}) \tag{10}$$

To consider the gravitational potential energies, the elevation of all mass centers must be considered. This can be represented as the static vector of torques/forces **G**, as

$$\mathbf{G}=-(\mathbf{J}_{v_1}^T(m_1\mathbf{g})+\mathbf{J}_{v_2}^T(m_2\mathbf{g})+.....+\mathbf{J}_{v_n}^T(m_n\mathbf{g})) \tag{11}$$

where, **g** is the gravitational vector. According to Fig. 2, **g** is found to be

$$\mathbf{g}=[0\quad -9.81\quad 0]^T \tag{12}$$

Finally, the forces related to centrifugal and Coriolis effects are considered as **V** vector, using (13).

$$\begin{aligned}
&\mathbf{c}_{kj}=\sum_{i=1}^{n}\mathbf{c}_{ijk}(\mathbf{q})\dot{\mathbf{q}}_i=\sum_{i=1}^{n}\frac{1}{2}\left\{\frac{\partial\mathbf{M}_{kj}}{\partial\mathbf{q}_i}+\frac{\partial\mathbf{M}_{ki}}{\partial\mathbf{q}_j}-\frac{\partial\mathbf{M}_{ij}}{\partial\mathbf{q}_k}\right\}\\
&\mathbf{V}=\mathbf{c}\dot{\mathbf{q}}
\end{aligned} \tag{13}$$

Considering **τ** as the vector of forces and torques related to the general coordinates, the dynamic model of the robot is derived as (14).

$$\mathbf{M}(\mathbf{q})\ddot{\mathbf{q}}+\mathbf{V}(\mathbf{q},\dot{\mathbf{q}})+\mathbf{G}(\mathbf{q})=\boldsymbol{\tau} \tag{14}$$

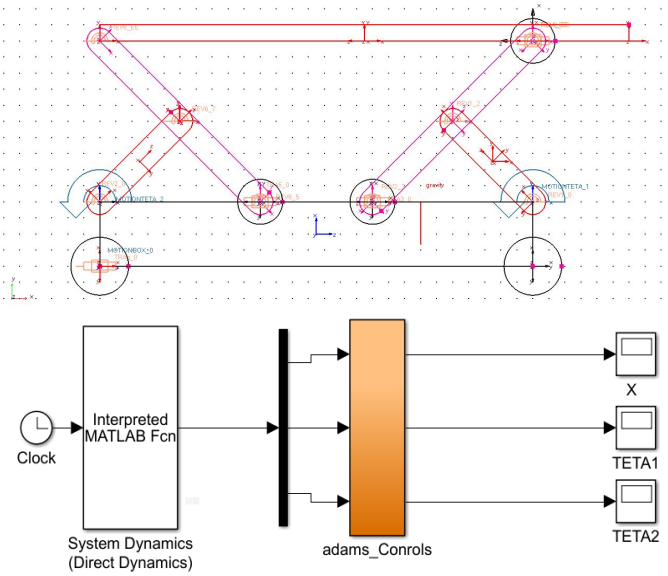

Fig. 3 Dynamic Model Validation; (up) Dynamic simulation by Adams software, (down) Adams Model Block in Simulink Matlab,

III. Dynamic Model Validation

In this section, the derived dynamic model is validated using software simulation. For software simulation, ADAMS™ is used. The robot is modeled in the software, as represented the Fig. 3(up). For comparison, the ADAMS model is exported to MATLAB Simulink as in Fig. 3(down). For validation, four robot motions were simulated. For each motion simulation, a predefined motion is given to the ADAMS model, as the input. Next, the required motor forces/torques are read as the simulation output. Finally, the results are compared with the model from (14), [26, 27].

In order to use ADAMS simulator, first, the models of all robot links are built it the software, including mass and inertia and dimension of each link. Next, all of the constraints, forces, torques and motions must be defined and added to the model. Since our model calculations are performed in MATLAB, the ADAMS model is exported to MATLAB Simulink, [28, 29].

A. First simulation:

As the first simulation, the robot is only moved forward and backward, in the x-direction, while the links do not rotate. The robot motion is considered as follows.

$$\mathbf{q} = \begin{bmatrix} 0.3\times\sin(0.2\times\pi\times t) & 0 & 0 \end{bmatrix}^T \tag{15}$$

The resulting forces, achieved from the ADAMS model and the mathematical model, are depicted and compared in Fig. 4.

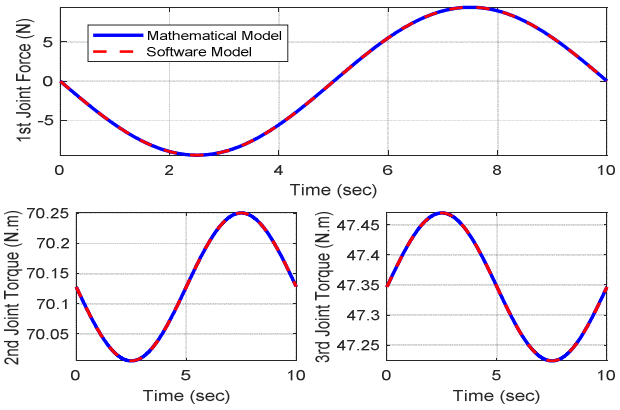

Fig. 4 Comparison of results from Adams model and the derived mathematical model in the first test.

B. Second simulation:

For the second test, only the front scissor motor moves, while the other motors are fixed. The motion is described as (16).

$$\mathbf{q} = \begin{bmatrix} 0 & 0.3\times\sin(\frac{4\pi t}{3}) & 0 \end{bmatrix}^T \tag{16}$$

The results for validation are depicted in Fig. 5.

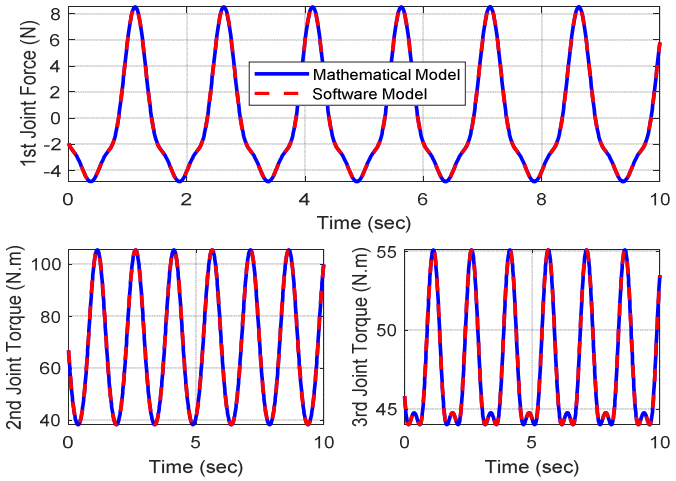

Fig. 5 Comparison of the results of the Second Test

C. The third simulation

In this test, only the rear scissor motor works, while the other motors are fixed. The motion is described as (17).

$$\mathbf{q} = \begin{bmatrix} 0 & \frac{\pi}{4} & \frac{\pi}{4} - 0.3\sin(\pi t) \end{bmatrix}^T \tag{17}$$

The results of this test are depicted in Fig. 6.

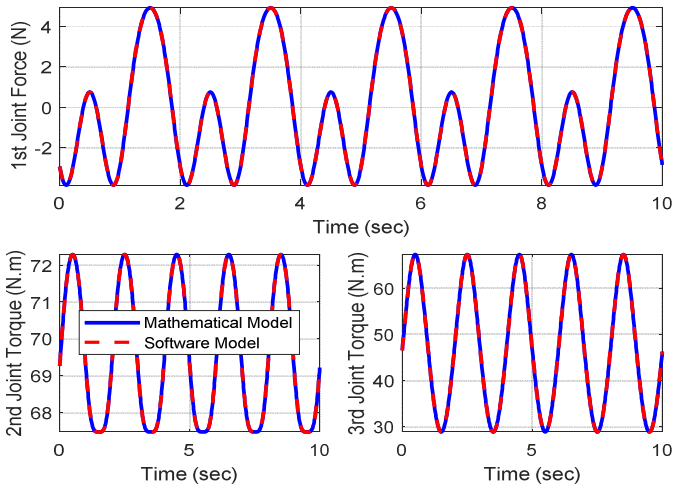

Fig. 6 Comparison results of the third test.

D. Fourth simulation:

For the last test, motions are given to all motors. Each motor has a motion with different frequency, as determined in (18).

$$\mathbf{q} = \begin{bmatrix} (0.3\times\sin(0.2\pi t) & \frac{\pi}{4} + 0.3\times\sin(\frac{4\pi t}{3}) & \frac{\pi}{4} - 0.3\times\sin(\pi t) \end{bmatrix}^T \tag{18}$$

The results achieved from the last simulation are depicted in Fig. 7.

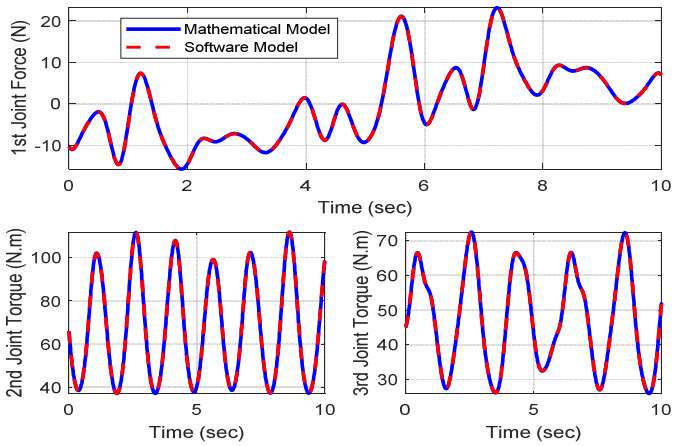

Fig. 7 Comparison results of the Fourth Test.

IV. PID CONTROL

As mentioned before, we have two main goals for the presented dynamic modeling. One goal is to analyze the prototype design before its manufacturing. The other goal is to study the prototype performance in control applications, which can also be used for motor selection, before manufacturing. To this end, a PID control diagram is presented, as depicted in Fig. 8. In this controller, the table position and orientation (the End Effector) are considered as the controller goals, which are assumed to be measured accurately by sensors. The system has three inputs, which are the forces and torques of the three motors. Using these motors, the three robot degrees of freedom can be controlled.

The model is nonlinear, with three inputs and three outputs. To design the PID coefficients, first, the model is simplified for each of its degrees of freedom. Then, using Ziegler-Nichols tuning method, the controller coefficients are chosen, and the tuned by try and error method, to achieve the proper settling times and reducing the overshoots. The controller coefficients for the three coordinates of the robot are shown in Table 1. A detailed discussion on the sensors, controller design and electromotor selection will be presented in another paper, including the limitations and requirements of the desired motion of the robot in a solar power plant, working with the delicate solar panels. For more realistic design, a saturation limit was considered for each motor. The saturation limit of the first motor is considered 150 N, and for the scissor motors 150 N.m.

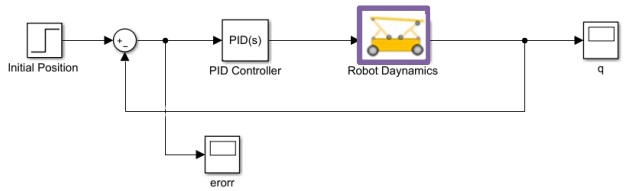

Fig. 8 Block diagram of the desired PID control robot

Table 1 The PID Controls coefficients for the three inputs

PID_x		
k_I	k_D	k_p
0.09	80	30
PID_{θ_1}		
k_I	k_D	k_p
800	100	500
PID_{θ_2}		
k_I	k_D	k_p
800	100	500

To investigate the performance of the proposed controller, a control task is defined and simulated. The initial position of the robot is considered as $\mathbf{q}_0$ and the desired position of the robot, represented $\mathbf{q}_{\text{des}}$, are considered as (19).

$$\mathbf{q}_0 = \begin{bmatrix} 0 & \frac{\pi}{2} & \frac{\pi}{2} \end{bmatrix}^T, \qquad \mathbf{q}_{des} = \begin{bmatrix} 6 & \frac{\pi}{4} & \frac{\pi}{4} \end{bmatrix}^T \tag{19}$$

Using the validated dynamic model, the controlled robot is simulated. The results are depicted in Fig. 9.

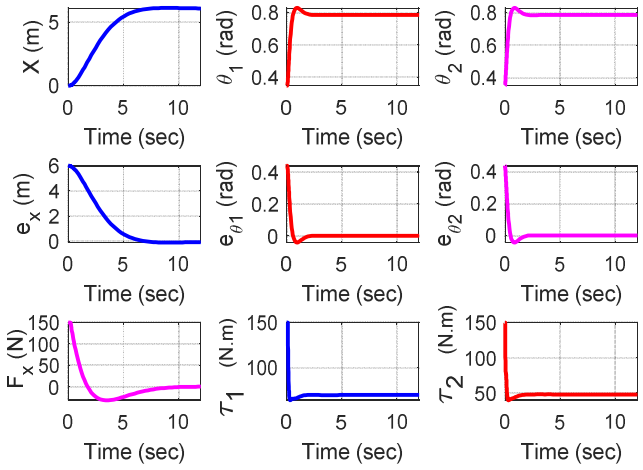

Fig. 9 Results of the PID controller simulation; (UP) diagrams of $(\boldsymbol{x}.\boldsymbol{\theta_1}.\boldsymbol{\theta_2})$; (middle) diagrams of errors; (down) torques and force.

V. CONCLUSION

This paper presented modeling and control of a robotic transportation system, for the cleaner unit used in solar power plants. First, the system geometry, its parameters and the kinematic modeling were presented. Then, the Lagrange method was used to derive the dynamic model of the robot. For validation, the robot was also modeled in ADAMS. The results achieved from ADAMS and the presented dynamic model were compared. Four tests were simulated and the comparison of results proves the validity of the proposed model. The main reasons of this robot modeling are to study the robot performance for the prototype design and also the design of its motors, based on the simulated performance in a control task. Hence, after modeling, a PID controller was proposed and designed, for position control of the robot. To study the

controller performance, a control simulation was presented, using MATLAB Simulink and ADAMS co-simulation. The achieved results of the control simulation show satisfactory performance of the proposed system.

REFERENCES

[1] E. De Schepper, S. Van Passel, J. Manca, and T. Thewys, "Combining photovoltaics and sound barriers–A feasibility study," Renewable energy, vol. 46, pp. 297-303, 2012.

[2] C. Dupraz, H. Marrou, G. Talbot, L. Dufour, A. Nogier, and Y. Ferard, "Combining solar photovoltaic panels and food crops for optimising land use: towards new agrivoltaic schemes," Renewable energy, vol. 36, no. 10, pp. 2725-2732, 2011.

[3] A. Syafiq, A. Pandey, N. Adzman, and N. A. Rahim, "Advances in approaches and methods for self-cleaning of solar photovoltaic panels," Solar Energy, vol. 162, pp. 597-619, 2018.

[4] N. M. Kumar, K. Sudhakar, M. Samykano, and S. Sukumaran, "Dust cleaning robots (DCR) for BIPV and BAPV solar power plants-A conceptual framework and research challenges," Procedia Computer Science, vol. 133, pp. 746-754, 2018.

[5] A. Goetzberger and A. Zastrow, "On the coexistence of solar-energy conversion and plant cultivation," International Journal of Solar Energy, vol. 1, no. 1, pp. 55-69, 1982.

[6] "Ministry of Energy Renewable Energy and Energy Efficiency Organization(ABA). SolarPowerPlant - SollarCraneirParsian; ; [cited 2019 Aug]. Available from: http://WWW/fa/list/solarpowerplants/cornercorpsolarcorp-." (accessed.

[7] J. Burgaleta, A. Ternero, D. Vindel, I. Salbidegoitia, and G. Azcarrraga, "Gemasolar, key points for the operation of the plant," SolarPACES, Marrakech, 2012.

[8] Bushong and S, "Robot Cleans Solar Panels And Protects Efficiency". Dust Wars " 2013.

[9] D. Deb and N. L. Brahmbhatt, "Review of yield increase of solar panels through soiling prevention, and a proposed water-free automated cleaning solution," Renewable and Sustainable Energy Reviews, vol. 82, pp. 3306-3313, 2018.

[10] Mr. Ashish Saini, Abhishek Nahar, Amit Yadav, Arnim, Dhruvash Singh Shekhawat, and M. A. Vijayvargiya, "Solar Panel Cleaning System," vol. 3, no. 5, 2017.

[11] A. K. Mondal and K. Bansal, "A brief history and future aspects in automatic cleaning systems for solar photovoltaic panels," Advanced Robotics, vol. 29, no. 8, pp. 515-524, 2015.

[12] "Serbot Swiss Innovations. GEKKO Solar Robot; [cited 2019 Aug]. Available from: http://WWW/en/solar-panels-cleaning/gekko-solar-robot." (accessed.

[13] M. Anderson et al., "Robotic device for cleaning photovoltaic panel arrays," in Mobile Robotics: Solutions and Challenges: World Scientific, 2010, pp. 367-377.

[14] "Ecoppia. EMPOWERING SOLAR; [cited 2019 Aug]. Available from: http://WWW/products-and-services/." (accessed.

[15] A. Ebrahimy, P. Zarafshan, S. R. Hassan-Beygi, M. Dehghani, and S. E. H. Garmdareh, "Design and Analysis of a Solar Linear Move Irrigation System," in RSI/ISM International Conference on Robotics and Mechatronics (ICRoM 2018), Tehran, Iran, 2018.

[16] M. Dehghani and S. A. A. Moosavian, "Modeling and control of a planar continuum robot," in Advanced Intelligent Mechatronics (AIM), 2011 IEEE/ASME International Conference on, 2011, pp. 966-971.

[17] M. Dehghani and S. A. A. Moosavian, "Compact modeling of spatial continuum robotic arms towards real-time control," Advanced Robotics, vol. 28, pp. 15-26, 2014.

[18] M. Dehghani and S. A. A. Moosavian, "Dynamics Modeling of a Continuum Robotic Arm with a Contact Point in Planar Grasp," Journal of Robotics, vol. 2014, p. 13, 2014.

[19] M. Dehghani and S. A. A. Moosavian, "Characteristics identification of continuum robots for exact modeling," in First RSI/ISM International Conference on Robotics and Mechatronics (ICRoM 2013), Tehran, Iran, 2013, pp. 26-31.

[20] M. Dehghani and S. A. A. Moosavian, "Modeling of continuum robots with twisted tendon actuation systems," in First RSI/ISM International Conference on Robotics and Mechatronics (ICRoM 2013), Tehran, Iran, 2013, pp. 14-19.

[21] M. Dehghani and M. Mahjoob, "A Modified Serpenoid Equation for Snake Robots," in IEEE International Conference on Robotics and Biomimetics (ROBIO 2008), Bangkok, Tailand, 2009, pp. 1647-1652.

[22] M. A. Jaradat et al., "A fully portable robot system for cleaning solar panels," in 2015 10th International Symposium on Mechatronics and its Applications (ISMA), 2015: IEEE, pp. 1-6.

[23] D.-C. Tranca, D. Rosner, and A.-V. Palacean, "Autonomous flexible low power industrial IoT controller for solar panels cleaning systems," in 2017 21st International Conference on Control Systems and Computer Science (CSCS), 2017: IEEE, pp. 106-112.

[24] John J. Craig, Introduction to Robotics Mechanics and Control. 3rd ed.

[25] Mark W. Spong, Seth Hutchinson, and M. Vidyasagar, Robot Modeling and Control. 1st ed.

[26] N. Azami, P. Zarafshan, A. M. Kermani, M. Khashehchi, and S. Kouravand, "Design and analysis of an armed-octorotor to prune trees near the power lines," in Int. conf. of Iranian aerospace society, 2017.

[27] M. Hafezipour, E. Saffari, P. Zarafshan, and S. A. A. Moosavian, "Manipulation control of multi-body free-floating space robot based on software combination," in 2013 First RSI/ISM International Conference on Robotics and Mechatronics (ICRoM), 2013: IEEE, pp. 271-276.

[28] S. R. Larimi, P. Zarafshan, and S. A. A. Moosavian, "Stabilized supervising control of a two wheel mobile manipulator," in 2013 First RSI/ISM International Conference on Robotics and Mechatronics (ICRoM), 2013: IEEE, pp. 265-270.

[29] F. Cheraghpour, M. Vaezi, H. E. S. Jazeh, and S. A. A. Moosavian, "Dynamic modeling and kinematic simulation of Stäubli© TX40 robot using MATLAB/ADAMS co-simulation," in 2011 IEEE International Conference on Mechatronics, 2011: IEEE, pp. 386-391.